Journal of Molecular Catalysis A: Chemical 299 (2009) 44–52

Contents lists available at ScienceDirect

Journal of Molecular Catalysis A: Chemical

journal homepage: www.elsevier.com/locate/molcata

Durable Ni/MgO catalysts for CO_2 reforming of methane: Activity and metal–support interaction

Yu-He Wang[a,b], Hong-Mei Liu[a], Bo-Qing Xu[a,*]

[a] *Innovative Catalysis Program, Key Lab of Organic Optoelectronics and Molecular Engineering, Department of Chemistry, Tsinghua University, Beijing 100084, China*
[b] *Department of Chemistry, Harbin Normal University, Harbin 150080, China*

ARTICLE INFO

Article history:
Received 27 July 2008
Received in revised form
16 September 2008
Accepted 23 September 2008
Available online 5 October 2008

Keywords:
Ni/MgO catalyst
Metal-support interaction
NiO–MgO solid solution
CO_2 reforming of methane
Catalyst stability

ABSTRACT

Two series of Ni/MgO catalysts were prepared by reducing NiO/MgO samples of fixed Ni loading but different calcination temperatures and of varying Ni loadings but fixed calcination temperature. These catalysts were investigated in CO_2 reforming of methane under atmospheric pressure and characterized with XRD, TPR and H_2-TPD techniques. A complete incorporation of NiO into the MgO "support" to form NiO–MgO solid solution during the calcination stage of the catalyst preparation was identified essential for the formation of stable Ni/MgO catalysts, and the presence of readily reducible "free" NiO in the calcined (unreduced) NiO/MgO samples was shown to produce the deactivating Ni/MgO catalysts during the CO_2/CH_4 reaction. The reactivities of CO_2/CH_4 were found sensitive to the particle size (or dispersion) of metallic Ni; the catalytic activity by CH_4 turnover frequency (TOF) decreased with increasing the Ni particle size. The reduced catalysts showed two H_2-TPD peaks and the nickel sites corresponding to H_2-TPD peak at higher temperature showed a higher activity than those associated with the peak at lower temperature. Our data demonstrate that the support in the stable catalysts was actually a kind of $Ni_xMg_{1-x}O$ ($x = 0.02$–0.15) solid solution and the stable catalytic sites were associated with nanosized Ni particles (3–20 nm) in strong interaction with the solid solution support..

1. Introduction

Compared with steam reforming of methane (STM) and partial oxidation of methane (POM), CO_2 reforming of CH_4 (CRM) provides an effective route for coinstantaneous conversion of two green house gases, CO_2 and CH_4, into valuable feedstocks with a suitable H_2/CO ratio for methanol syntheses [1–2]. Great efforts have been made on the development of highly active and stable catalysts for CRM reaction [3–5]. Over the past decades, Ni/MgO catalyst reduced from NiO–MgO solid solution has been attracting renewed interest due to its high stability in CRM reaction [6–13]. Fujimoto et al. prepared and studied $Ni_{0.03}Mg_{0.97}O$ solid solution for the CRM reaction. They showed that the catalytic activity of this $Ni_{0.03}Mg_{0.97}O$ catalyst remained stable over 100 days [6–8]. Ruckenstein and Hu investigated the catalytic performances of reduced NiO–MgO solid solutions, which were prepared by impregnation and subsequent calcination at 800 °C, with a NiO content in the range of 4.8–50.0 wt% [9–11]. They found that catalysts containing 9.2–28.6 wt% NiO showed stable activity. However, no activity was observed over the catalyst with NiO content as low as 4.8 wt%. And, the catalyst with a high NiO content of 50.0 wt% deactivated rapidly because of the sintering of Ni particles and severe coke formation. The authors suggested that the excellent activity and high stability of the reduced NiO–MgO catalyst depended on their composition, preparation conditions and the properties of the MgO support (surface area, pore size distribution and lattice parameters). An unsuitable MgO would lead to a low initial conversion and a long induction period for the reaction [12]. In an exploratory work using MgO nanocrystals for support of the nickel catalysts, our laboratory showed that a loading of 12 wt% Ni onto MgO nanocrystals, which were produced by thermal processing of a $Mg(OH)_2$ alcogel in flowing nitrogen, can lead to highly active and stable Ni/MgO catalyst for the CO_2 reforming of methane [13].

It is indicated that NiO and MgO can form theoretically "ideal" solid solution in any molar ratio [14–16]. However, the formation of NiO–MgO solid solution is much influenced by the preparation conditions, such as calcination temperature, loading amount of nickel, and so on [17–19]. Reducibility of Ni^{2+} in NiO–MgO solid solution depends on the position of Ni^{2+} in MgO lattice and the interaction between Ni^{2+} and MgO [19]. For the Ni/MgO catalyst reduced from NiO–MgO solid solution, the interaction between metallic Ni and support would be affected by the preparation history of the

* Corresponding author. Fax: +86 10 6279 2122.
E-mail address: bqxu@mail.tsinghua.edu.cn (B.-Q. Xu).

1381-1169/$ – see front matter © 2008 Elsevier B.V. All rights reserved.
doi:10.1016/j.molcata.2008.09.025

NiO–MgO solid solution. The intrinsic relationship between the extent of NiO incorporation in the solid solution and the catalytic performance of its derived Ni/MgO catalyst has not yet been fully understood.

In the earlier studies of CRM reaction over supported metals catalysts, CH_4 (or CO_2) conversion was generally used as a parameter to evaluate the activity of a catalyst [20,21]. Actually, CH_4 conversion is significantly affected by the feed gas hourly space velocity (GHSV) and the amount of active metal on the reduced catalyst. Comparatively, the activity can be distinctly clarified by measuring CH_4 turnover frequency (TOF) on the metallic active sites. In several investigations, TOF numbers of CH_4 were estimated and used as standard to describe the activity of a catalyst [22–26]. Unfortunately, the majority of these TOF numbers was obtained by using low GHSVs, which effected CH4 conversion levels too close to the thermodynamic equilibrium of the reversible CRM reaction, where the rate of reverse reaction is comparable with the forward one, and therefore, the "actual activity" of the active Ni sites in CRM reaction remains unclear. Thus, it is necessary to perform the CMR reaction with an enough high GHSV to eliminate the constraint of thermodynamic equilibrium and obtain the "true" TOF of methane conversion, as suggested by Parmaliana et al. [22].

In this work, the calcination temperature and NiO loading in NiO/MgO samples were independently varied to better understand how the formation of NiO–MgO solid solution in the calcined NiO/MgO sample would affect the activity and stability of its derived Ni/MgO catalyst. By measuring the catalytic TOF of CH4 under very high GHSV, we established a correlation between the intrinsic activity of metallic Ni sites and the particle size of Ni in the reduced Ni/MgO catalysts

2. Experimental

2.1. Catalyst preparation

Magnesia support was prepared by thermal processing a $Mg(OH)_2$ alcogel in flowing nitrogen at 650 °C for 5 h. The $Mg(OH)_2$ alcogel was obtained from a $Mg(OH)_2$ hydrogel by washing with anhydrous ethanol for several times. Detailed preparation of the hydrogel was described previously [13]. The oxidized NiO/MgO samples were prepared by wet impregnating an suitable amount of $Ni(NO_3)_2$ aqueous solution onto the MgO nanocrystals. In our previous work, magnesia prepared in this method was denoted as MgO-AN and the prepared catalyst Ni/MgO-AN [27–29]. After impregnation and drying at 120 °C for 12 h, two series samples were prepared as following. In one series, the dried samples with a Ni loading of 8.8 wt% were calcined in air for 5 h at a temperature in the range from 400 to 950 °C, while in other series, the samples with different loading of Ni in the range of 3.4–45.0 wt% were calcined at 650 °C for 5 h in air. The final loading amounts of nickel in the samples were determined by XRF analysis. The calcined samples were denoted as NiαMg-*T*, where α is the Ni loading in weight percentage, and *T* is the calcination temperature in degree Celsius.

2.2. Catalyst characterizations

A Bruker D8 Advance X-ray Diffractometer (XRD) with Cu *K*α radiation (λ = 0.15406 nm) was used to identify the crystal phases in the samples. The operation voltage was 40 kV and the current was 40 mA. The XRD patterns were recorded with a resolution of 0.02° and a scan rate of 0.3 s/point.

Quantitative temperature-programmed reduction (TPR) experiments were conducted on a homemade TPR equipment to determine the reducibility of samples. About 200 mg of sample was placed in a quartz reactor and reduced by a 5% H_2/Ar mixture in a flow rate of 50 ml/min. The temperature was ramped at 15 °C/min up to 850 °C and held for 1 h. Before reduction, the samples were purged with pure argon at 600 °C for 30 min. Water, which is the only volatile product of the reduction, was removed with a cold trap at −80 °C to avoid its interference to TCD detector that was used to record the hydrogen consumption. The TPR measurement was followed by a H_2-TPD to measure the chemisorption of hydrogen. After TPR measurement, the sample was cooled to room temperature in 5% H_2/Ar mixture and held for 1 h. The sample was then purged at room temperature with pure Ar (50 ml/min) for removing the reversibly adsorbed H_2. When the baseline of TCD became stabilized, the sample was heated at a rate of 15 °C/min up to 800 °C in pure Ar (50 ml/min). The signal of H_2 desorption recorded by a

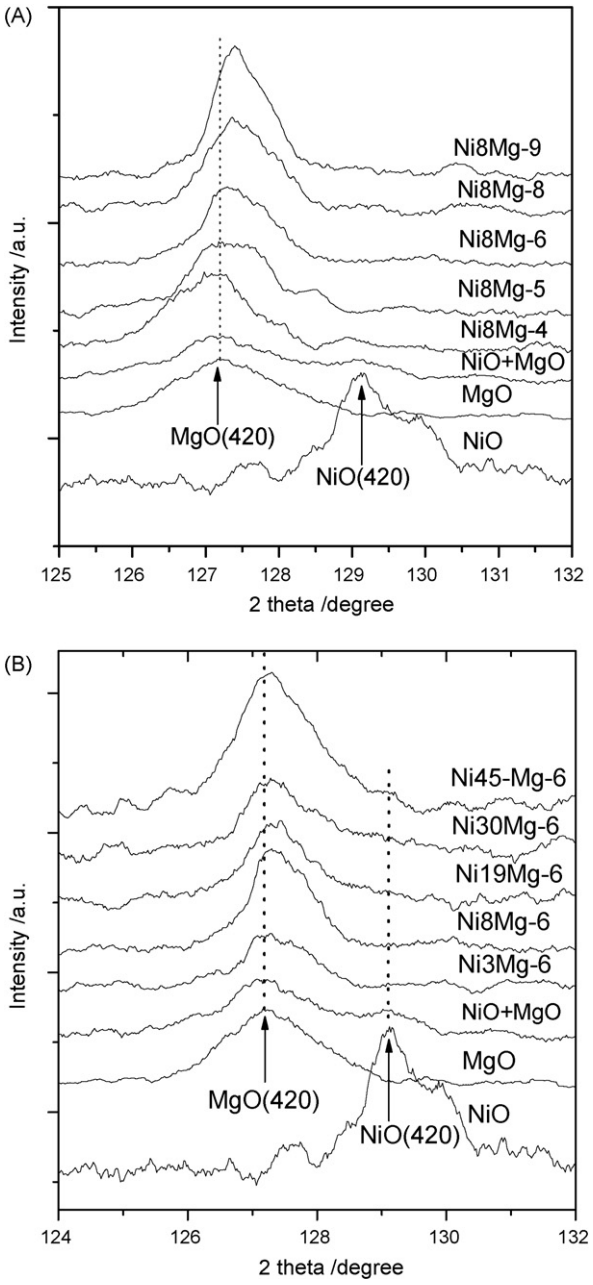

Fig. 1. XRD patterns of NiO/MgO samples with fixed Ni loading (8.8 wt% Ni) but different calcination temperatures (400–950 °C) (A); and with varying Ni loading (3.4–45.0 wt%) but fixed calcination temperature (650 °C) (B).

computer and the ratio of 2 × (area of TPD-area)/(area of TPR-area) gave the dispersion of reduced nickel. The average particle size of metallic Ni was calculated according to an empirical equation: d (nm) = 1/dispersion [13].

2.3. Activity test

The CRM reaction was carried out using 100 mg NiO/MgO sample (20–40 mesh) under conditions: CH_4:CO_2 = 1:1 (molar ratio), 750 °C, 0.1 MPa, and feed GHSV = 1.6×10^4–2.4×10^5 ml g^{-1} h^{-1} in a fixed-bed quartz tubular reactor (7 mm i.d.). Prior to the reaction, the sample was reduced in situ with flowing 5% H_2/Ar mixture in a flow rate of 50 ml/min. The temperature was ramped at 15 °C/min up to 850 °C and held for 1 h. Reaction products were analyzed with an on-line gas chromatograph (Varian 3400) equipped with a thermal conductivity detector. Preliminary experiments have been carried out by changing the flowing rate of the feed gas mixture and the grain size of the solid catalyst to investigate the diffusion effect, which showed that the reactant conversions were not significantly affected by either internal or and external diffusion when the reactant GHSV was in the range of 1.6×10^4–2.4×10^5 ml g^{-1} h^{-1} in this work.

3. Results

3.1. XRD results

According to literature [30] and our recent works [27–29], it is more sensitive to distinguish the diffraction peak of NiO, MgO and NiO–MgO solid solution at $2\theta > 100°$ with XRD technique. Fig. 1 shows the XRD patterns of pure NiO, MgO and mechanical mixture NiO + MgO (8.8 wt% Ni), as well as calcined Ni8Mg-T and NiαMg-6 samples in a 2θ angle range of 124–132°, the corresponding 2θ values of each sample are given in Table 1. It has been known that the diffraction peaks of MgO would slightly shift to higher angles when Ni^{2+} ions diffuse into MgO lattice while the diffraction peaks of NiO would slightly shift to lower angles with the diffusion of Mg^{2+} into NiO lattice [30]. The physical mixture of NiO + MgO powder showed the individual XRD peaks at 127.30° and 129.16°, respectively, just as the standard peaks of MgO(4 2 0) and NiO(4 2 0). This showed that any interaction between Ni^{2+} ions and the MgO lattice was insignificant in the physical mixture of NiO + MgO powder [30]. From Fig. 1A and Table 1, it can be seen that NiO(4 2 0) diffraction peak in the XRD pattern of Ni8Mg-4 appeared at 128.94°, lower than the diffraction angle of pure NiO(4 2 0). This indicates the occurrence of Mg^{2+} diffusing into NiO lattice, thus "free" NiO or NiO-based NiO–MgO solid solution may exist in Ni8Mg-4. Meanwhile, the diffraction peak of MgO(4 2 0) also shifted from 127.30° for the pure MgO(4 2 0) to a higher angle of 127.34°, giving an evidence of the occurrence of Ni^{2+} diffusing into MgO lattice to form MgO-based NiO–MgO solid solution [30,31]. In XRD pattern of Ni8Mg-5, the diffraction peaks of NiO(4 2 0) and MgO(4 2 0) appeared at 128.50° and 127.38°, respectively, also showing the existence of "free" NiO or NiO-based MgO–NiO solid solution and the MgO-based NiO–MgO solid solution. With increasing calcination temperature up to ≥650 °C, no diffraction peaks of NiO(4 2 0) were observed in the XRD profiles of Ni8Mg-6, Ni8Mg-8 and Ni8Mg-9 samples, suggesting that all of the loaded NiO in the samples were incorporated into the MgO "support" to form NiO–MgO solid solution.

XRD patterns of NiαMg-6 samples are shown in Fig. 1B. The absence of NiO(4 2 0) peak in the XRD patterns of samples with Ni loadings in the range of 3.4–30.2 wt% revealed that no "free" or NiO-based MgO–NiO was present in the samples. This indicated that all of the Ni^{2+} ions were incorporated into the lattice of MgO "support" to form NiO–MgO solid solution. For the Ni45Mg-6 sample, an obvious NiO diffraction peak appeared at 129.14°, which showed almost the same angle with pure NiO, indicating the presence of "free" NiO or NiO-based MgO–NiO solid solution. For each one of the samples, the diffraction peak of MgO shifted from 127.30° up to 127.40°, indicating the formation of a MgO-based NiO–MgO solid solution due to the incorporation of Ni^{2+} into the lattice of the MgO "support".

3.2. TPR results

Fig. 2 shows the TPR profiles of pure NiO, Ni8Mg-T (Fig. 2A) and NiαMg-6 (Fig. 2B) samples. The temperatures of TPR peaks and NiO reducibility are listed in Table 2. The peaks observed at temperatures lower than 500 °C was denoted as T_L, 500–750 °C as T_M and the other peak at a temperature higher than 800 °C was marked as T_H. The T_M peaks are usually assigned to the reduction of Ni^{2+} ions in the outermost layer and sub-surface layers of the MgO lattice, while the T_H peaks can be attributed to the reduction of Ni^{2+} ions in the MgO matrix [31]. The presence of these T_M and T_H peaks are clear symbols of the formation of NiO–MgO solid solution. As shown in Fig. 2A, NiO in the Ni8Mg-4 and Ni8Mg-5 samples did not diffused completely into MgO to form NiO–MgO solid solution. Whereas, NiO in the other samples calcined at temperatures higher than 650 °C was completely incorporated into the "support" to form NiO–MgO solid solution. These results were consistent with the XRD measurements (see Fig. 1A).

Fig. 2B shows that NiO in Ni45Mg-6 was also not completely incorporated into MgO to form NiO–MgO solid solution. The NiO in other NiaMg-6 samples with Ni loadings no higher than 30 wt%

Table 1
Composition, BET surface area and XRD diffraction angles for NiO(4 2 0) and MgO(4 2 0) planes of the calcined NiO/MgO samples.

Samples	Calcination temperature (°C)	Ni loading (%)	Composition of solid solution	Surface area (m^2 g^{-1})	XRD angle (2θ) (degree)	
					MgO(4 2 0)	NiO(4 2 0)
MgO	650	–	–	59	127.30	–
NiO	650	–	–	–	–	129.16
Ni8Mg-4	400	8.8	75.0% NiO/$Ni_{0.015}Mg_{0.985}O$	56	127.34	128.94
Ni8Mg-5	500	8.8	22.0% NiO/$Ni_{0.050}Mg_{0.950}O$	52	127.38	128.50
Ni8Mg-6	650	8.8	$Ni_{0.064}Mg_{0.936}O$	48	127.40	n.d[a]
Ni8Mg-8	800	8.8	$Ni_{0.064}Mg_{0.936}O$	36	127.44	n.d.
Ni8Mg-9	950	8.8	$Ni_{0.064}Mg_{0.936}O$	24	127.46	n.d.
Ni3Mg-6	650	3.4	$Ni_{0.024}Mg_{0.976}O$	53	127.40	n.d
Ni8Mg-6	650	8.8	$Ni_{0.064}Mg_{0.936}O$	48	127.40	n.d.
Ni19Mg-6	650	19.3	$Ni_{0.15}Mg_{0.85}O$	40	127.40	n.d
Ni30Mg-6	650	30.2	$Ni_{0.25}Mg_{0.75}O$	38	127.40	n.d
Ni45Mg-6	650	45.0	7.0% NiO/$Ni_{0.38}Mg_{0.62}O$	36	127.40	129.14

[a] Not detectable.

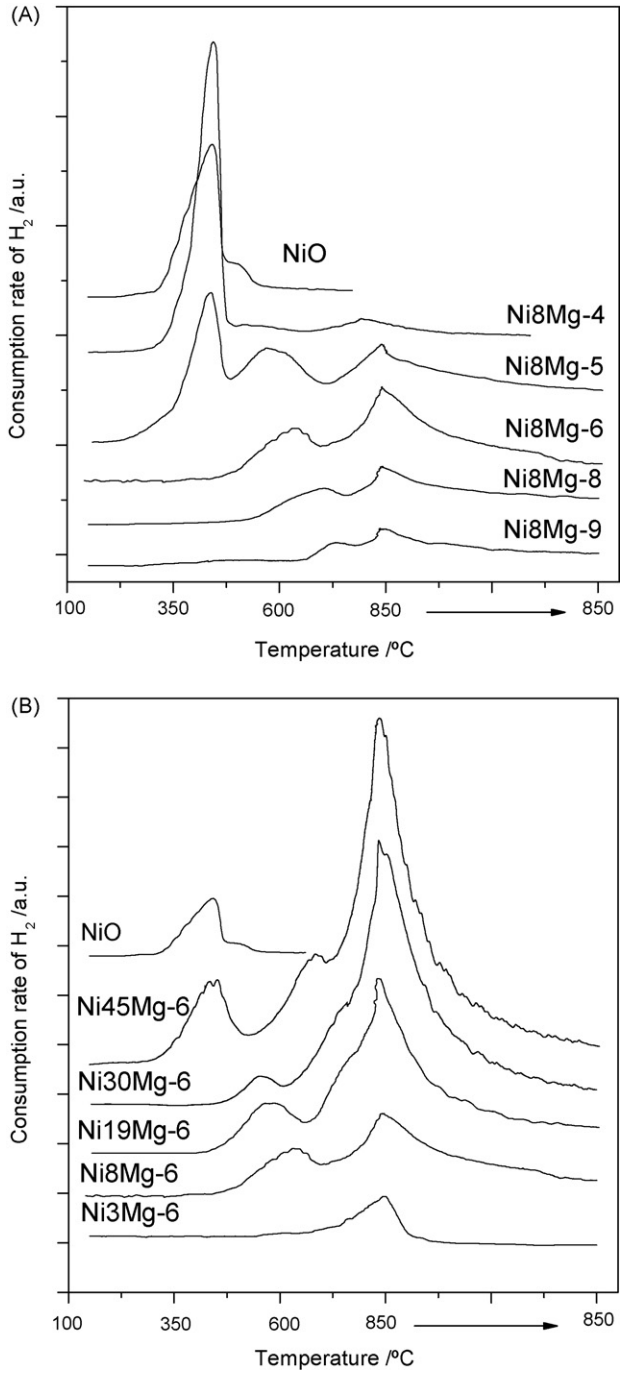

Fig. 2. TPR profiles of the calcined NiO/MgO samples with fixed Ni loading (8.8 wt% Ni) but different calcination temperatures (400–950 °C) (A); and with varying Ni loading (3.4–45.0 wt%) but fixed calcination temperature (650 °C) (B).

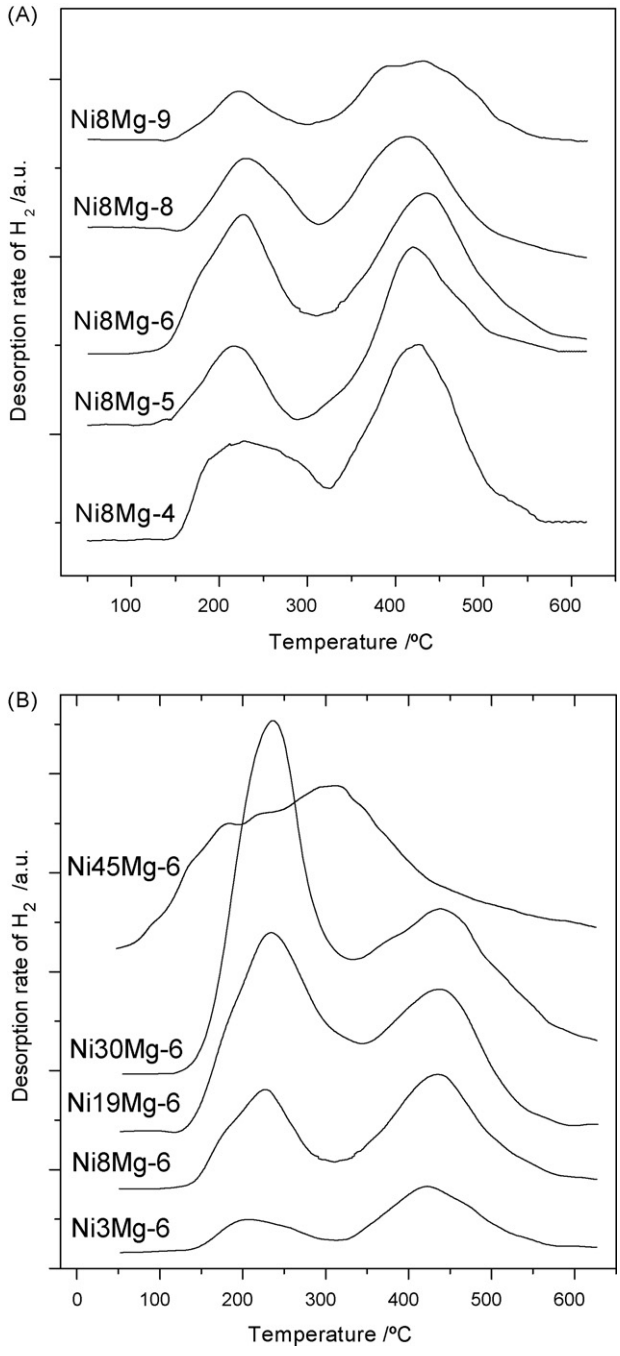

Fig. 3. H_2-TPD profiles of freshly reduced Ni8Mg-*T* (A) and (B) NiαMg-6 catalysts.

was completely converted into the NiO–MgO solid solution. These results were also consistent with the XRD measurements (see Fig. 1B).

Since the NiO in NiO–MgO solid solution could not be completely reduced at the temperature used in this of our work (i.e., 850 °C) the actual support in the reduced catalyst should be better called/described as a kind of NiO–MgO solid solution, thus the reduced Ni/MgO catalyst can be more reasonably expressed as $Ni_x/Ni_yMg_{1-y}O$ (see Table 2). Where, *x* and *y*, respectively, were the calibrated amount of the reduced and unreduced nickel in the reduced samples.

3.3. H_2-TPD measurements

Fig. 3 shows the H_2-TPD profiles from the reduced Ni8Mg-*T* and NiαMg-6 catalysts. On the basis of TPR and H_2-TPD measurements, the number of exposed Ni atoms, the exposed percentage (dispersion) and particle size of the metallic Ni were calculated and listed in Table 3. Every sample in this table, except Ni45Mg-6, featured two peaks at about 230 and 435 °C, respectively. This demonstrated an involvement of two types of Ni sites for hydrogen chemisorption on each catalyst. For convenience, the two types of Ni sites were denoted as θ_1 and θ_2 (see Table 3) according to the desorption temperatures of hydrogen from them. The relative areas of the H_2-TPD peaks were used to estimate the relative numbers θ_1 to θ_2

Table 2
Reducibility of NiO/MgO samples and composition of reduced Ni/MgO catalysts by TPR measurements.

Samples	Peak temperature (°C)			Reducibility (%)	Composition of reduced catalysts
	T_L	T_M	T_H		
NiO	450	–	–	–	–
Ni8Mg-4	455	–	810	84	$Ni_{0.056}/Ni_{0.01}Mg_{0.99}O$
Ni8Mg-5	455	580	850	50	$Ni_{0.033}/Ni_{0.033}Mg_{0.967}O$
Ni8Mg-6	–	650	850	24	$Ni_{0.015}/Ni_{0.050}Mg_{0.950}O$
Ni8Mg-8	–	710	850	14	$Ni_{0.009}/Ni_{0.055}Mg_{0.945}O$
Ni8Mg-9	–	740	850	7	$Ni_{0.005}/Ni_{0.059}Mg_{0.941}O$
Ni3Mg-6	–	–	850	18	$Ni_{0.004}/Ni_{0.02}Mg_{0.98}O$
Ni8Mg-6	–	650	850	24	$Ni_{0.015}/Ni_{0.050}Mg_{0.950}O$
Ni19Mg-6	–	580/720	850	36	$Ni_{0.06}/Ni_{0.10}Mg_{0.90}O$
Ni30Mg-6	–	570/730	850	47	$Ni_{0.14}/Ni_{0.15}Mg_{0.85}O$
Ni45Mg-6	460	700	850	53	$Ni_{0.29}/Ni_{0.25}Mg_{0.75}O$

sites, which are shown as θ_1/θ_2 in the last column of Table 3. For the preparation of NiO–MgO solid solutions without "excessive" or "free" NiO at a fixed Ni loading (e.g., 8.8% Ni), the increase of the calcination temperature from 650 to 950 °C (e.g., Ni8Mg-6, -8 and -9 samples) caused the θ_1/θ_2 ratio to decrease from 0.78 to 0.41 and the Ni particle size to decrease from 6.7 to 2.9 nm. For the samples with varying Ni loadings in the calcined solid solutions, the θ_1/θ_2 ratio increased from 0.45 to 2.11, while the Ni particle size increased from 3.2 to 20.0 nm when the Ni loading was increased from 3.4 to 30.2 wt%. These results imply that the θ_1 Ni sites were prevalent on large Ni particles while the θ_2 Ni sites were dominant on the small Ni particles in the reduced catalysts.

As it was shown in the last section of this paper, a part of NiO in the NiO–MgO solid solutions of the calcined samples remained as a constituent in the solid solution support of the final reduced catalysts (Table 2). These unreduced Ni^{2+} ions in the final support (i.e., $Ni_yMg_{1-y}O$) could induce stronger metal-support interaction in the final $Ni_x/Ni_yMg_{1-y}O$ catalysts than in conventional Ni/MgO ones. That is why for the $Ni_x/Ni_yMg_{1-y}O$ catalysts reduced from the NiO–MgO solutions without "free" NiO, the smaller the ratio of x/y, the smaller the particle size of the Ni metal (Tables 2 and 3). The reduction of NiO in the NiO–MgO solid solution could also lead to a number of defects at the support surface to "anchor" the metallic Ni particles, which would easily result in stable Ni sites resistant to sintering and coking for the demanding CRM reaction.

It should be noticed that the ratios of θ_1/θ_2 for the reduced Ni8Mg-4 and Ni8Mg-5 as well as the Ni45Mg-6 samples that were prepared from calcined NiO/MgO precursors containing more or less "free" NiO entities, are against the change trend of the θ_1/θ_2 ratios with the Ni particle size. A very broad hydrogen desorption feature, probably involving two unresolved peaks at ca. 200 and 300 °C, was detected in the temperature range of 50–500 °C on the H_2-TPD profile of the reduced Ni45Mg-6 catalyst, as shown in Fig. 3B. Although two clear peaks appeared also on the H_2-TPD profiles of the reduced Ni8Mg-4 and Ni8Mg-5 catalysts, the metallic sites on the reduced Ni8Mg-4 and Ni8Mg-5 catalysts seem to be dissimilar with those on the other catalysts. TPR results have indicated the existence of "free" NiO on these three exceptive catalysts. Maybe, the Ni particles reduced from the "easily reducible" NiO were different from those reduced from the "hardly reducible" NiO–MgO solid solution. This question needs a further investigation.

3.4. Catalytic performance of the reduced catalysts

The catalytic dry reforming of methane was performed at atmospheric pressure and 750 °C, with a stoichiometric feed of CH_4 and CO_2. Fig. 4 shows the effect of feeds GHSV on CH_4 conversion over the reduced Ni8Mg-6 catalyst. This catalyst showed very stable activity in CO_2 reforming of methane not only with a low GHSV (1.6×10^4 ml g^{-1} h^{-1}), but also with a rather high GHSV (2.4×10^5 ml g^{-1} h^{-1}). The CH_4 conversion obtained by using the lowest GHSV (1.6×10^4 ml g^{-1} h^{-1}) was 84%, just close to the equilibrium conversion of methane at 750 °C (86%). As expected, the CH_4 conversion decreased with increasing GHSV. When the GHSV was increased to 1.2×10^5 and 2.4×10^5 ml g^{-1} h^{-1}, the CH_4 conversions decreased to 36% and 29%, respectively. The invariant CH_4 conversion levels in the 50 h reaction TOS under these high feed GHSVs clearly demonstrate the catalyst stability under conditions far away from the thermodynamic equilibrium of the reaction, revealing a realization of the steady state of the catalytic kinetics.

Fig. 5 shows the TOF numbers of CH_4 calculated on the basis of exposed metallic Ni atoms (listed in Table 3) and the methane conversion data under the different GHSVs. The TOF of CH_4 increased from 1.5 to 4.7 s^{-1} with increasing the GHSV from 1.6×10^4 to 9.6×10^4 ml g^{-1} h^{-1}, and was kept unchanged when

Table 3
Exposed percentage (dispersion) and particle size of metallic Ni, number of exposed Ni atoms and the ratio of active Ni sites determined from H_2-TPD measurements.

Reduced catalysts	H_2-TPD peak temperature (°C)		Dispersion (%)	Ni size[a] (nm)	Exposed Ni (μmol g^{-1})	θ_1/θ_2[b]
	θ_1	θ_2				
Ni8Mg-4	230	425	6	16.7	78	0.54
Ni8Mg-5	225	430	10	10.0	74	0.41
Ni8Mg-6	230	435	15	6.7	52	0.78
Ni8Mg-8	230	425	22	4.5	46	0.62
Ni8Mg-9	225	430	34	2.9	37	0.41
Ni3Mg-6	220	430	31	3.2	33	0.45
Ni8Mg-6	230	435	15	6.7	52	0.78
Ni19Mg-6	230	435	7	14.3	84	1.61
Ni30Mg-6	235	440	5	20.0	113	2.11
Ni45Mg-6	50–500	3	33.3	135	–	

[a] Ni size (nm) calculated according to the empirical equation: d (nm) = 1/dispersion.
[b] Ratio of active Ni sites associated with the two H_2-TPD peaks.

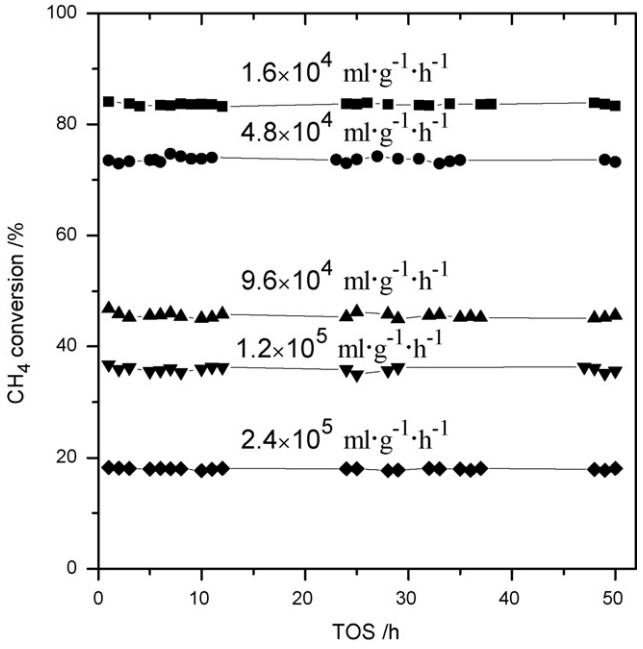

Fig. 4. CH_4 conversion versus reaction time for CH_4/CO_2 reaction at 750 °C with different feed GHSV (1.6×10^4–2.4×10^5 ml g^{-1} h^{-1}) over reduced Ni8Mg-6 catalyst.

the reaction GHSV was further increased up to 2.4×10^5 ml g^{-1} h^{-1}. This observation clearly demonstrates that those TOF numbers of CH_4 measured at GHSVs lower than ca. 1.0×10^5 ml g^{-1} h^{-1} or CH_4 conversion levels higher than 40% was not reliable, due to significant influence of the reverse reaction. And, reliable intrinsic TOF numbers of CH_4 over the reduced Ni/MgO catalysts can be obtained under real kinetic conditions, when the GHSV was enough high and CH_4 conversion was enough low. Thus, the other Ni/MgO catalysts were evaluated for the CRM reaction under an enough high GHSV (i.e., 1.2×10^5 ml g^{-1} h^{-1}) to measure and compare the intrinsic activity of metallic Ni sites by CH_4 TOF.

Fig. 6 shows the effects of calcination temperature and Ni loading on the catalytic performance of Ni/MgO catalyst at 750 °C with

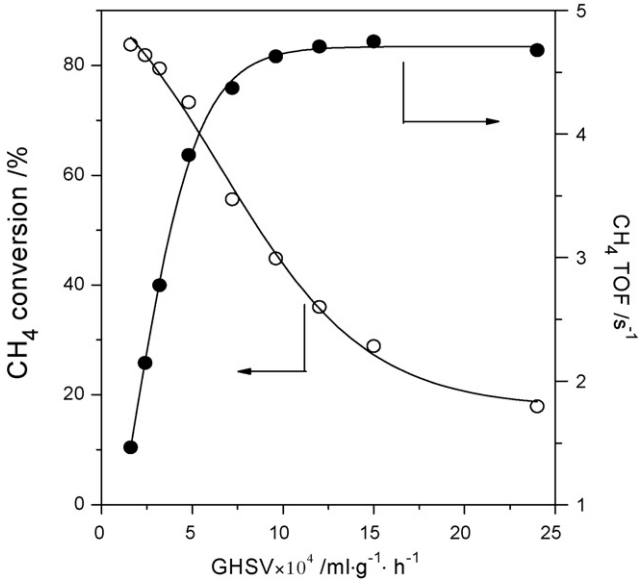

Fig. 5. CH_4 conversion and CH_4 TOF versus feed GHSV for CH_4/CO_2 reaction at 750 °C over reduced Ni8Mg-6 catalyst.

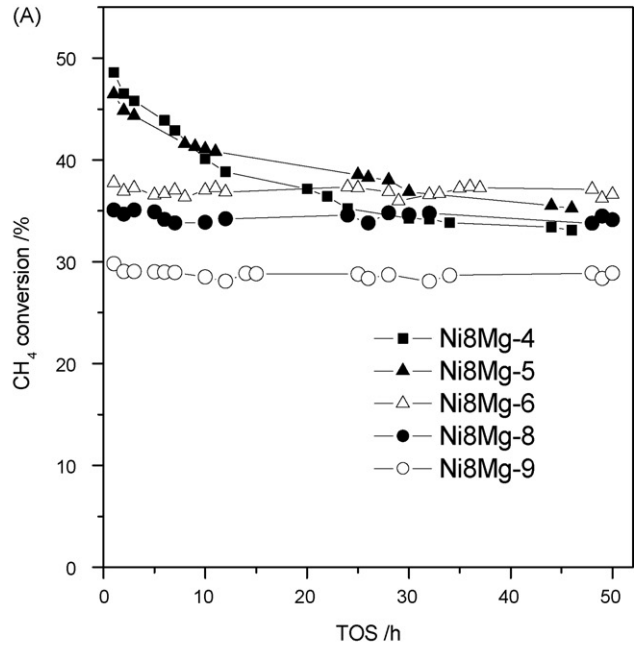

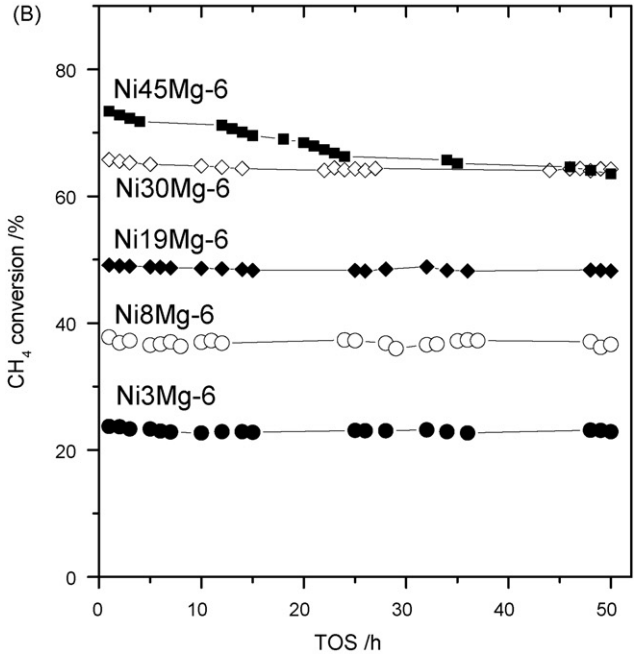

Fig. 6. Catalytic stability by CH_4 conversion for CH_4/CO_2 reaction at 750 °C and 1.2×10^5 ml g^{-1} h^{-1} over Ni8Mg-*T* (A) and NiαMg-6 catalysts (B).

a GHSV of 1.2×10^5 ml g^{-1} h^{-1}. All of the reduced Ni8Mg-*T* and NiαMg-6 catalysts showed very stable activity for the CH_4/CO_2 reaction, except for the reduced Ni8Mg-4, Ni8Mg-5 and Ni45Mg-6 catalysts that contained in their oxidized states some unreacted "free" NiO particles. With decreasing the calcination temperature or increasing the Ni loading in the process of catalyst preparation, the initial CH_4 conversions increased for the two series of Ni/MgO catalysts.

4. Discussion

It was documented earlier that when all NiO particles diffuse into MgO lattice to form a NiO–MgO solid solution, the reduced

catalyst would show stable activity in the CRM reaction [12]. The catalytic reaction rate or TOF of CH_4 would be dependent of the number of exposed metallic nickel atoms as well as the size and shape of Ni particles in the reduced catalyst [21]. Changes in the preparation conditions, i.e. calcination temperature, Ni loading, etc. of a Ni/MgO catalyst can adjust and control the formation of NiO–MgO solid solution and the metal-support interaction in the final reduced catalyst. The present data are in line with these earlier understandings on the catalytic activity and stability of the reduced Ni/MgO catalyst. On the other hand, our data also showed that the stable Ni catalysts were actually produced by incomplete reduction of NiO in the NiO–MgO solid solutions; the "real" support of the stable Ni catalysts was a kind of NiO–MgO solid solution (i.e., $Ni_yMg_{1-y}O$, Table 2). Thus, it would be interesting to correlate the extent of NiO incorporation in the MgO "support" or the percentage of NiO in the solid solution of the calcined catalyst precursor with the metal-support interaction and catalytic performance of the reduced $Ni_x/Ni_yMg_{1-y}O$ catalysts.

4.1. Effect of metal–support interaction on the catalytic stability of the reduced catalyst

Both XRD and TPR results (Figs. 1 and 2 and Tables 1 and 2) showed the formation of NiO–MgO solid solution in the calcined samples. Nevertheless, the extent of NiO incorporation in the NiO–MgO solid solution depended on the calcination temperature and the Ni loading. All of the NiO diffused and became incorporated into the MgO phase to form the NiO–MgO solid solution, when the calcination temperature was not lower than 650 °C and the Ni loading was in the range of 3.4–30.2 wt%. Whereas, on the samples calcined at a lower temperature (e.g., 400 or 500 °C) or with a higher Ni loading (e.g., 45.0 wt%), only a part of NiO could be incorporated into the lattice of the MgO "support", and the excessive NiO remained in a form of "free" NiO. Only a fraction of Ni^{2+} ions in the calcined samples could be reduced to form metallic Ni particles, though the sample with a lower calcination temperature and/or a higher Ni loading showed a higher reducibility of Ni^{2+} (see Table 2). The reduced Ni8Mg-4, Ni8Mg-5 and Ni45Mg-6 catalysts, whose calcined precursor samples contained NiO–MgO solid solution as well as "free" NiO phases, showed significant deactivation, while the other catalysts, whose calcined precursor samples contained the NiO–MgO solid solution phase only, exhibited quite stable activities during the CH_4/CO_2 reaction (see Fig. 6).

The metallic Ni particles in the deactivating Ni/MgO catalysts were formed from reduction of the "free" NiO and a part of NiO in the NiO–MgO solid solution of the calcined Ni8Mg-4, Ni8Mg-5 and Ni45Mg-6 samples. The so-called "free" NiO in these samples showed less interaction with their underlying support and was reduced at much lower temperatures (Fig. 2) than its counterparts in NiO–MgO solid solution. Such easily reducible "free" NiO would lead to Ni sites having much weaker metal-support interaction, which could be responsible for the deactivation of the reduced Ni8Mg-4, Ni8Mg-5 and Ni45Mg-6 catalysts. It is noted that the deactivation rate of the reduced Ni8Mg-5 catalyst was slower than that of the reduced Ni8Mg-4 as shown in Fig. 6A. Since these two samples had the same Ni loading (8.8 wt%), their difference in the percentages of "free" NiO (75% in Ni8Mg-4 and 22% in Ni8Mg-5, see Table 1) would suggest that the catalyst deactivation rate was dependent of the percentage of NiO (or Ni^{2+}) incorporation in NiO-MgO solid solution of the calcined sample; the higher the percentage of Ni^{2+} incorporation the higher the catalytic stability of the reduced catalyst. When all of the loaded Ni^{2+} ions (or NiO) were incorporated into the lattice of the MgO "support" during the calcination step in the catalyst preparation, the reduction with H_2 at 850 °C always produced metallic Ni sites showing stable catalytic activities for the CRM reaction (Fig. 6), indicating that a NiO–MgO solid solution without any "free" NiO is a key to the very stable Ni/MgO (or $Ni/Ni_yMg_{1-y}O$) catalyst. The Ni particles formed from such a reductive partial extraction of Ni^{2+} ions in the solid solution would have strong enough interaction with the $Ni_yMg_{1-y}O$ support to resist the sintering and to depress the deposition of carbon on the reduced catalysts [12].

Hu and Ruckenstein [12] also observed that the reducibility of NiO in calcined NiO/MgO increased with increasing the Ni loading. As a result, the particle size of metallic Ni would also increase with the Ni loading and would became too large to resist sintering and coking at high Ni loadings [12]. They thus suggested that the large Ni particles in Ni/MgO catalyst of high Ni loading were the main cause for Ni sintering, coke formation and catalyst deactivation during the CRM reaction [12]. However, according to the present data (Table 3 and Fig. 6), the particle size of metallic Ni was not the only affecting factor on the catalytic stability of the reduced Ni/MgO catalyst. The size of Ni particles on reduced Ni30Mg-6 (20.0 nm) was much larger than those on reduced Ni8Mg-4 and Ni8Mg-5 (16.7 and 10.0 nm, respectively), as shown in Table 3. However, the Ni30Mg-6 catalyst showed very stable activity, but the Ni8Mg-4 and Ni8Mg-5 catalysts deactivated rapidly in the CH_4/CO_2 reaction. These results indicated that not only the loading of Ni and Ni particle size in the reduced catalyst but also physicochemical state of NiO in the oxidized sample affected the stability of the reduced catalyst. That is to say that it would be impossible to obtain stable Ni sites for the CRM reaction if one reduces an oxidized/calcined NiO/MgO precursor containing NiO entities that are not belong to the NiO–MgO solid solution. Therefore, a complete reaction of the NiO component with the "supporting" MgO during the calcination step to form a NiO–MgO solid solution phase is the key to the preparation of stable Ni/MgO catalyst. The incomplete reduction of NiO from the solid solution would produce Ni sites that interact strongly with a $Ni_yMg_{1-y}O$ support. This $Ni_yMg_{1-y}O$ support can be considered as deficient NiO–MgO solid solution featuring a number of Ni^{2+} defects. It is suggested that these defects played an important role in stabilizing the catalytic Ni sites for the CRM reaction.

4.2. Effect of metal–support interaction on CH_4 turnover frequency

In order to elucidate the effect of metal–support interaction on the initial rate of CH_4 conversion, we show in Fig. 7, the change trend of the initial CH_4 TOF (i.e., CH_4 TOF measured in the initial 20 min of the reaction) with the Ni particle size on the two series of Ni/MgO catalysts, which covered a relatively wide Ni particle size range (3.0–30.0 nm, see Table 3). Whether for the Ni8Mg-*T* or NiαMg-6 catalysts, the TOF of methane conversion increased with decreasing the Ni particle size. Thus, the catalytic activity expressed by the TOF of CH_4 is of the function TOF = f (Ni size) for the two series of Ni/MgO catalysts, revealing that the catalytic activity (CH_4 TOF) of metallic Ni at the beginning of the reaction was related with the Ni particle size, but not the calcination temperature or Ni loading. The relationship also suggests indicated that the reaction of CRM over reduced Ni/MgO catalyst was strongly structure-sensitive. A similar observation was documented earlier for Ni/MgO catalyst in the CH_4/H_2O reaction (i.e., steam reforming of methane) by Parmaliana et al. [22].

4.3. CH_4 turnover frequency on different Ni sites

In order to correlate the energy state of different Ni sites on the reduced catalysts with their steady state catalytic activity in the CRM reaction, the steady state CH_4 TOF is plotted in Fig. 8 against the fraction of θ_1 sites, which is equivalent to the fractional area

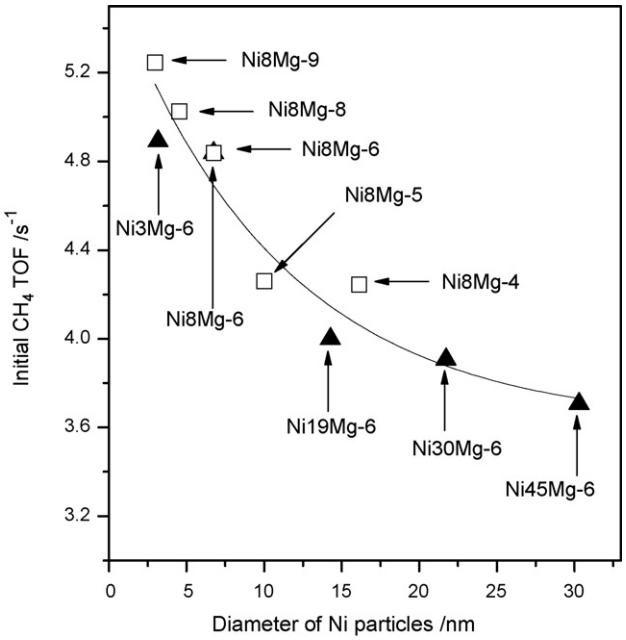

Fig. 7. CH_4 TOF versus Ni particle size for CH_4/CO_2 reaction at 750 °C and 1.2×10^5 ml g^{-1} h^{-1} over Ni8Mg-*T* (□) and NiαMg-6 catalysts (▲).

of the low temperature hydrogen desorption peak (θ_1 peak) on the H_2-TPD profiles in Fig. 3. This low temperature (*ca.* 230 °C) θ_1 peak can be attributed to the hydrogen desorption from the low-index planes and terraces at the surface of metallic Ni particles. And, the θ_2 peak at higher temperature (*ca.* 435 °C) can be attributed to the hydrogen desorption from the step and kink sites at the surface of metallic Ni particles. The CH_4 TOF decreased with increasing the fraction of θ_1 sites, as shown in Fig. 8. This correlation indicates that the θ_1 sites are less active than the θ_2 sites in the CRM reaction. With reference to the Ni particle sizes shown in Table 3, it is concluded that small Ni particles (ca. 3.0 nm) in strong interaction with the

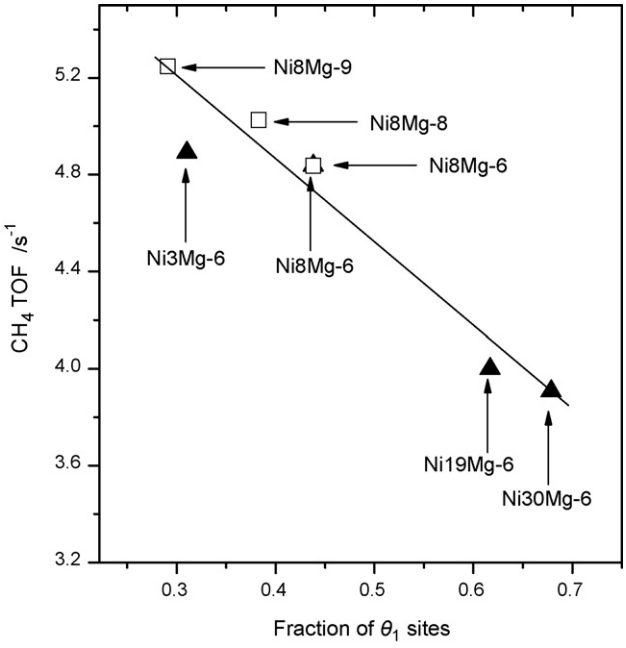

Fig. 8. CH_4 TOF versus the fraction of θ_1 sites for CH_4/CO_2 reaction at 750 °C under a feed GHSV of 1.2×10^5 ml g^{-1} h^{-1} over Ni8Mg-*T* (□) and NiαMg-6 catalysts (▲).

solid solution $Ni_yMg_{1-y}O$ support are most active and yet stable for the CRM reaction.

Szuromi et al. investigated the C–H bond activation of methane on model metal surfaces and concluded that the C–H bond dissociation was a kinetically relevant step in methane conversion and occurred faster on step and kink sites than on terrace sites of metal particles [33]. Density functional theory has also been used to understand the activation of methane on Rh-based model catalyst. It was found that the activation energy of CH_4 on the step and kink sites was about 30 kJ/mol lower than that on close-packed terrace planes [32]. Wei and Iglesia investigated the turnover rates of CH_4 for the forward reactions of CH_4/H_2O, CH_4/CO_2 and CH_4 decomposition reactions on Al_2O_3 or ZrO_2 supported Rh of various dispersions. They found that the methane turnover rates increased as the particle size of Rh supported on Al_2O_3 or ZrO_2 decreased. They also suggested that the coordinatively unsaturated surface atoms prevalent in small crystallites were significantly more active than those in the low-index planes predominately exposed on large crystallites [25,26].

It should be mentioned, however, that the relationship shown in Fig. 8 is not applicable to the reduced Ni45Mg-6, Ni8Mg-4 and Ni8Mg-5 catalysts. Perhaps, the involvement of Ni sites from the the reduction of "free" NiO in the calcined/oxidized catalyst precursor would lead to less defects in the final $Ni_yMg_{1-y}O$ support, which would then weaken the metal-support interaction in the reduced catalyst to favor metal sintering and coking during the reaction. This point needs a further investigation.

5. Conclusions

The present data showed that a complete reaction of the NiO component with "supporting" MgO to form a solid solution $Ni_xMg_{1-x}O$ phase ($x = 0.06$–0.25) during the calcination of NiO/MgO precursors is the key to stable Ni/MgO catalysts for the CRM reaction. The support in the stable catalyst was actually a kind of $Ni_yMg_{1-y}O$ ($y = 0.02$–0.15) solid solution and the stable catalytic sites were associated with nanosized Ni particles (3–20 nm) in strong interaction with the solid solution support. The catalytic activity by methane turnover frequency increased with decreasing the Ni particle size. The reduction of an oxidized/calcined NiO/MgO precursor containing NiO entities that were not incorporated into the $Ni_xMg_{1-x}O$ solid solution was shown to produce the deactivating catalyst.

Acknowledgments

The authors thank the Natural Science Foundation (NSF) of China (grant: 20590360) and the National Basic Research Program of China (grant: 2003CB615804) for financial support of this work.

References

[1] M.C.J. Bradford, M.A. Vannice, Catal. Rev. Sci. Eng. 41 (1999) 1–42.
[2] S.B. Wang, G.Q. Lu, Energy Fuels 12 (1998) 248–256.
[3] L. Pelletier, D.D.S. Liu, Appl. Catal. A 317 (2007) 293–298.
[4] G.S. Gallego, F. Mondragón, J. Barrault, J.M. Tatibouët, C. Batiot-Dupeyrat, Appl. Catal. A 311 (2006) 164–171.
[5] H. Sun, H. Wang, J. Zhang, Appl. Catal. B 73 (2007) 158–165.
[6] Y.G. Chen, K. Tomishige, K. Fujimoto, Chem. Lett. (1997) 999–1000.
[7] Y.G. Chen, K. Tomishige, K. Yokoyama, K. Fujimoto, Appl. Catal. A 165 (1997) 335–347.
[8] K. Tomishige, O. Yamazaki, Y.G. Chen, K. Yokoyama, X.H. Li, K. Fujimoto, Catal. Today 45 (1998) 35–39.
[9] E. Ruckenstein, Y.H. Hu, Appl. Catal. A 133 (1995) 149–161.
[10] Y.H. Hu, E. Ruckenstein, Catal. Lett. 43 (1997) 71–77.
[11] Y.H. Hu, E. Ruckenstein, Catal. Lett. 36 (1996) 145–149.
[12] Y.H. Hu, E. Ruckenstein, Catal. Rev. Sci. Eng. 44 (2002) 423–453.
[13] B.Q. Xu, J.M. Wei, H.Y. Wang, K.Q. Sun, Q.M. Zhu, Catal. Today 68 (2001), 217-215.

[14] A. Zecchina, G. Spoto, S. Coluccia, E. Guglielminotti, J. Chem. Soc. Faraday Trans. I 80 (1984) 1891–1901.
[15] T. Yoshida, T. Tanaka, H. Yoshida, T. Funabiki, S. Yoshida, J. Phys. Chem. 100 (1996) 2302–2309.
[16] J.G. Highfield, A. Bossi, F.S. Stone, Preparation of Catalysts III, Elsevier, Amsterdam, 1983.
[17] N. Takezawa, H. Terunuma, M. Shimokawabe, H. Kobayashi, Appl. Catal. 23 (1986) 291–298.
[18] A. Parmaliana, F. Arena, F. Frusteri, N. Giordano, J. Chem. Soc. Faraday Trans. 86 (1990) 2663–2669.
[19] F. Arena, B.A. Horrell, D.L. Cocke, A. Parmaliana, N. Giordano, J. Catal. 132 (1991) 58–67.
[20] O. Yamazaki, K. Tomishige, K. Fujimoto, Appl. Catal. A 136 (1996) 49–56.
[21] E. Ruckenstein, H.Y. Wang, Catal. Lett. 73 (2001) 99–105.
[22] A. Parmaliana, F. Arena, F. Frusteri, S. Coluccia, L. Marchese, G. Martra, A.L. Chuvilin, J. Catal. 141 (1993) 34–47.
[23] H.Y. Wang, E. Ruckenstein, Appl. Catal. A 204 (2000) 143–152.
[24] J.Z. Luo, Z.L. Yu, C.F. Ng, C.T. Au, J. Catal. 194 (2000) 198–210.
[25] J.M. Wei, E. Iglesia, J. Catal. 225 (2004) 116–127.
[26] J.M. Wei, E. Iglesia, J. Catal. 224 (2004) 370–383.
[27] Y.H. Wang, B.Q. Xu, Catal. Lett. 99 (2005) 89–96.
[28] Y.H. Wang, H. Wang, Y. Li, Q.M. Zhu, B.Q. Xu, Top. Catal. 32 (2005) 109–116.
[29] Y.H. Wang, H.M. Liu, B.Q. Xu, Chin. J. Catal. 26 (2005) 1117–1121.
[30] F. Arena, F. Frusteri, A. Parmaliana, L. Plyasova, A.N. Shmakov, J. Chem. Soc. Faraday Trans. 92 (1996) 469–471.
[31] F. Arena, A. Licciardello, A. Parmaliana, Catal. Lett. 6 (1990) 139–150.
[32] Z.P. Liu, P. Hu, J. Am. Chem. Soc. 125 (2003) 1958–1967.
[33] P.D. Szuromi, J.R. Engstrom, W.H. Weinberg, J. Phys. Chem. 89 (1985) 2497–2502.